energies

MDPI

Review

Reduction of Iron Oxides for CO_2 Capture Materials

Antonio Fabozzi *, Francesca Cerciello and Osvalda Senneca *

National Research Council, Institute of Sciences and Technologies for Sustainable Energy and Mobility (CNR-STEMS), P. le V. Tecchio 80, 80125 Napoli, Italy; francesca.cerciello@stems.cnr.it
* Correspondence: antonio.fabozzi@stems.cnr.it (A.F.); osvalda.senneca@stems.cnr.it (O.S.)

Abstract: The iron industry is the largest energy-consuming manufacturing sector in the world, emitting 4–5% of the total carbon dioxide (CO_2). The development of iron-based systems for CO_2 capture and storage could effectively contribute to reducing CO_2 emissions. A wide set of different iron oxides, such as hematite (Fe_2O_3), magnetite (Fe_3O_4), and wüstite ($Fe_{(1-y)}O$) could in fact be employed for CO_2 capture at room temperature and pressure upon an investigation of their capturing properties. In order to achieve the most functional iron oxide form for CO_2 capture, starting from Fe_2O_3, a reducing agent such as hydrogen (H_2) or carbon monoxide (CO) can be employed. In this review, we present the state-of-the-art and recent advances on the different iron oxide materials employed, as well as on their reduction reactions with H_2 and CO.

Keywords: iron oxide; CO_2 capture; adsorption/desorption enhanced; hematite; magnetite; wüstite

1. Introduction

In the last few decades, CO_2 emissions have significantly increased, attracting the attention of the scientific community because these emissions are the main cause of the greenhouse effect [1,2]. The rise of the CO_2 concentration in the atmosphere is due to deforestation [3] and highly energetic industries, particularly in the sectors of chemicals [4], power, and steel, largely sustained by fossil fuels [5,6]. The steel industry alone is responsible for ~7% of the total CO_2 emission because of the wide use of fossil fuels [7,8].

Despite the increasing share of renewables for power generation and the acceleration towards the utilization of H_2 as a combustible in the steel industry [9,10], the International Energy Agency (IEA) reports that currently more than 80% of the world's energy is still based on fossil fuel combustion [11,12], and in a mid-term scenario all large scale/industrial plants should employ some type of equipment in order to reduce CO_2 emissions [13,14]. For this reason, a wide set of energy companies are developing and testing strategies of carbon capture and sequestration (CCS) [15,16]

CCS [17,18] includes the separation, liquefaction, and finally storage of CO_2. The CO_2 can be stored (i) in deep ocean masses, (ii) in deep geological formations, or (iii) in the form of carbonates [19,20]. The most promising sequestration sites are the geological formations due to the possibility of storing ~2000 Gigatons of CO_2 [21,22]. In particular, the injection of CO_2 in oil reservoirs, mixed with different types of surfactants [23–27], is a validated technology to enhance oil recovery (EOR) [28,29]. Indeed, the combination based on the capture of CO_2 and its employment in EOR technology effectively reduces the CCS costs. Unfortunately, nowadays there are no power plants present that can operate with complete CCS methods because of the high cost and energy penalty of the capture stage, especially for hot and dilute flows derived from power plants [30,31]. Recent advances in research are primarily aimed at reducing costs and increasing the efficiency and selectivity of CO_2 separation and capture [32,33].

CO_2 capture technologies are based on either chemical [34] or physical methods [35]. In physical methods, CO_2 is adsorbed by a solid and is further released by decompression

check for updates

Citation: Fabozzi, A.; Cerciello, F.; Senneca, O. Reduction of Iron Oxides for CO_2 Capture Materials. *Energies* **2024**, *17*, 1673. https://doi.org/10.3390/en17071673

Academic Editor: Nikolaos Koukouzas

Received: 28 February 2024
Revised: 22 March 2024
Accepted: 28 March 2024
Published: 1 April 2024

and/or heating under different conditions of temperature and pressure [36,37]. Contrariwise, the chemical methods are based on chemical reactions between CO_2 and liquids, such as amine solutions, or reactive solid sorbents, such as CaO [38,39]. The current benchmark for CO_2 capture in coal, oil, or natural gas power plants and other heavy industrial processes is absorption with amine solutions [40–45], while calcium looping capture is one step back in the Technology Readiness Level (TRL) [46]. Unfortunately, capture with amine solutions is very energy-intensive and expensive [47,48]; indeed, amine systems are capable of capturing ~85% of the CO_2 from the exhaust gas of a fossil-fuel power plant but with a penalty of ~25% of the plant electricity production [49,50].

CO_2 capture with membranes is a more recent solution but does not yet represent a mature alternative to amine capture. Indeed, their convenience is hampered by the large amount of exhaust gas that has to be treated [51,52]. The scientific community is, in fact, focusing on the enhancement of CO_2-nitrogen (N_2) membrane selectivity by using the facilitated mechanism membranes [53,54].

Another approach which has been recently gaining a prominent role is the use of metal oxides, such as iron oxides, magnesium oxides (MgO), and calcium oxides (CaO), for CO_2 capture, via the formation of carbonates [55,56]. In the second step, carbonates can be heated up to release back pure CO_2 gas and regenerate metal oxides [57,58]. Overall a cyclic process can be set, which includes the exothermic carbonation reaction and the endothermic carbonate decomposition [59,60].

In this review, we discuss the prospects of iron oxides in the context of energy transition, with a particular focus on their application for CCS. The features of the different types of iron oxides and their suitability for CO_2 capture will be surveyed. The thermodynamic and kinetic aspects of iron oxides reduction with H_2 or CO are also addressed.

2. Iron Oxides in the Context of Energy Transition and CCS

2.1. Motivation for the Use of Iron Oxides in CCS

The use of iron in the context of CCS is particularly appealing thanks to its large availability across the globe [61–63] and relative economy.

Iron is present in the planet mainly as hematite (Fe_2O_3), magnetite (Fe_3O_4), and wüstite (FeO). Other iron-based compounds include sulfides, hydroxides, and carbonates [64–66].

Iron oxides have been proposed both for pre-capture processes, such as chemical-looping combustion (CLC) [67–69], and for post combustion CO_2 capture. CLC processes have been developed in order to increase the concentration of CO_2 in the exhaust gases, thus reducing the costs of post combustion CO_2 capture processes. The high concentration of CO_2 is attained by performing carbon oxidation in a *Fuel* reactor, where the airflow is replaced by recycled flue gas. Here the oxygen necessary for carbon oxidation is released from the metal oxygen carriers, in particular iron oxides, which reduce to iron. The latter is, then, re-oxidized in a reactor, named the *Air* reactor, and recycled back to the *Fuel* reactor.

As far as the post combustion capture applications are concerned, iron has been proposed for the preparation of enhanced sorbents and used in combination with carbonaceous supports. However, the simplest and probably most direct and economic way to exploit iron oxides, in particular Fe_2O_3 and Fe_3O_4, is for capturing CO_2 from exhaust gases through the formation of carbonates (siderite $FeCO_3$). The carbonation stage can be followed by a high temperature decarbonation step to regenerate iron and release gaseous CO_2. Such a solution appears particularly appealing for capturing CO_2 from steel plants, where iron powders (even waste) are available on site and can be profitably exploited. Iron carbonates can be regenerated through the decarbonation reaction either in the same facility [70], or at locations far from the CO_2 emission/capture sites.

In this context, another important advantage can be envisaged: siderites can be safely transported via trucks, allowing CO_2 transport without the need of pipelines. However, in the techno-economic analysis, it must be considered that for the transport of 44 ton of CO_2, approximately 116 ton of material (in the form of siderite) must be handled (for a ratio of 44/156 = 0.38 g/g, which can be compared with the values of 0.1–0.3 g/g reported

for CO_2 capture over metal organic frameworks (MOFs) [71]. Another issue that has to be considered for the economy of the process is that, in order to capture CO_2, the divalent or trivalent oxides of iron must be previously reduced in the metallic state [72,73] by a reduction agent, such as H_2 or CO. This step is crucial and might end up being the bottleneck of the process. This step will, indeed, be addressed in detail in the next paragraphs. Finally, the possibility of the utilization of iron materials over repeated cycles needs to be further investigated.

2.2. Hematite

Fe_2O_3 is one of the most important ores for industrial applications and represents 60%, of the iron ore reserve worldwide [74]. Oxygen (O_2) carriers using Fe_2O_3 as an active phase [75] or natural Fe_2O_3 have been widely investigated in the context of CLC. Notably, Al_2O_3 and SiO_2 in combination with Fe_2O_3, can further enhance the properties of O_2 carriers in CLC, their durability and reactivity [76].

Some studies investigated the use of Fe_2O_3 in natural ores and in waste materials as oxygen carriers in the CLC of fossil fuels, including coal and biomass with gas. Indeed, Zhang et al. studied the use of natural Fe_2O_3 in the CLC of coal under pressurized conditions and their results found no sintering on the Fe_2O_3 surface and good reaction performance [77]. Gu et al. used natural Fe_2O_3 [78] in the CLC of sawdust at 800 °C. Song et al. investigated the natural Fe_2O_3 CLC combustion of ShenHua bituminous coal and HuaiBei anthracite [79].

Furthermore, Fe_3O_4 and Fe_2O_3 can be employed as sorbents for CO_2 capture. Indeed, Mendoza et al. have investigated CO_2 capture and release employing Fe_2O_3 and Fe_3O_4. In particular, the chemical reactions among CO_2 and iron oxides were explored versus both the CO_2 pressure and ball mill process parameters. The experimental results indicated that the carbonation of iron oxides can be achieved at 10–30 bar and at room temperature. Furthermore, the complete calcination of $FeCO_3$, was investigated under Ar and vacuum atmospheres and it was found that at 367 °C $FeCO_3$ decomposed, yielding carbon and or ion and Fe_3O_4. In particular, it was highlighted that this mixture can reversibly capture CO_2 in several carbonation–calcination cycles [36].

2.3. Magnetite

Fe_3O_4 is an iron oxide widely employed as a component of industrial heterogeneous catalysts for its availability, stability, and low cost [80]. It has a spinel structure, and the mixed valence state, +2/+3, of the Fe can catalyze both acid–base and oxidation–reduction reactions [81]. For instance, in the Haber–Bosch process, Fe_3O_4 is part of the catalysts employed for ammonia production, in which Fe_3O_4 is reduced by H_2 to the active form α-Fe, allowing the adsorption and dissociation of the N_2 molecules [82].

In the last decade, in the CO_2 capture scenario, Fe_3O_4 has also been used to produce amine-functionalized nanofluids with higher CO_2 absorption rates than pure solvents [83]. Fe_3O_4 nanoparticles attracted scientific attention thanks to their low toxicity and high stability [84]. Park et al. have developed novel nano absorbents composed of Fe_3O_4 nanoparticles functionalized with different organic and inorganic materials such as (3-Aminopropyl) triethoxysilane (ATS), tetraethyl orthosilicate (TeOS), and L (+)-ascorbic acid (A). In order to synthesize an Fe_3O_4 double-functionalization, a primary coating with A followed by a secondary SiO_2 shell and subsequently, the amine functionalization by means of ATS was applied. The CO_2 absorption capacity of newly functionalized material, with A, was 11% higher than that of the un-functionalized ones, Fe_3O_4-SiO_2-NH_2. However, in order to determine the absorption improvement of functionalized material at 25 °C, concentrations ranging from 0.1 to 0.4 wt% were compared with those in which water was used as a reference. The highest CO_2 absorption improvement of 59.2% was achieved at a concentration of 0.3 wt% which is higher than blank Fe_3O_4, Fe_3O_4-A-SiO_2 at 0.3 wt%. Furthermore, a demonstration of cyclic performances was established in order to test its potential employment for industrial applications [85].

The observed enhancement of the CO_2 absorption of iron-amine-based nanofluids has been attributed to improved mass transfer compared to conventional amines solutions, thanks to a combination of effects [86]: the hydrodynamic effect [87,88], the shuttle effect [86,89], and the bubble-breaking effect [90,91]. However, these nanofluids still have limitations for industrial applications because they are susceptible to acid and oxidation conditions.

Furthermore, recently, a mechanochemical process aiming at capturing CO_2 by using Fe_2O_3 and Fe_3O_4 has been employed in the CO_2 capture field; this process led to the formation of $FeCO_3$ via carbonation reactions (1) and (2) [36].

$$Fe_3O_4(s) + Fe(s) + 4CO_2 \rightarrow 4FeCO_3(s) \quad (1)$$

$$Fe_2O_3(s) + Fe(s) + 3CO_2 \rightarrow 3FeCO_3(s) \quad (2)$$

In particular, Mendoza et al. [36], have investigated the ball milling condition effects (revolution speed, pressure, and reaction time) for both reactions (1) and (2) and found that the capturing capacity of the Fe_2O_3 and Fe system was higher than that of Fe_3O_4 and Fe at the same conditions of pressure, temperature, and reaction. In particular, the results demonstrated a capture capacity of 7.98 mmol CO_2 $g^{-1}_{sorbent}$ in 3 h at 200 °C and 10 bar CO_2 pressure. Furthermore, the oxides could be completely regenerated by applying an oxidation step at 350 °C under airflow [15].

2.4. Wüstite

Wüstite is not commonly found as a natural material but is an intermediate derived from the reduction of iron ores, Fe_2O_3 and Fe_3O_4. The chemical formula of wüstite is $Fe_{(1-y)}O$, where y is the relative number of the ferrous iron ion vacancies. The O_2 content can change at different temperatures from a 23.16 wt% to 25.60 wt% range in variation. $Fe_{(1-y)}O$ is thermodynamically unstable and prone to re-oxidize at ambient conditions; however, it can be also further reduced to metallic iron using agents such as carbon (C), CO, and H_2.

Recently O_2 carriers composed of $Fe_{(1-y)}O$ mixed with other oxides, such as those of manganese (Mn) have been used in the chemical looping combustion of coal. It has been found that a fraction of O_2 was transferred via an uncoupling mechanism [92]. Perèz-Vega et al. prepared particles starting from Mn_3O_4 and Fe_2O_3 powders with an atomic ratio fixed at Mn:Fe, 77:23 by a ball mill. Subsequently, the solids mixture was calcined for 4 h at 1050 °C, and the calcined solid was milled for 300 min. Furthermore, the material behavior was evaluated during both the decomposition–regeneration of the $[(Mn_{0.77}Fe_{0.23})_2O_3]$ phase, bixbyite, in chemical looping with O_2 uncoupling, and the reduction–oxidation of $[(Mn_{0.77}Fe_{0.23})_3O_4]$, spinel phase, with CO, H_2, and CH_4. In particular, the chemical looping combustion redox cycle, using gaseous fuels, highlighted high reactivity with CO and H_2 and high O_2 transport capacity due to the reduction of $[(Mn_{0.77}Fe_{0.23})O]$, mangano-wüstite phase. Therefore, this material is considered a promising candidate to be employed in CLC with both coal and gas [93].

Furthermore, even if the wüstite is not stable, it has been used in combination with MgO in order to increase the CO_2 capture capability of MgO sorbents. Chen et al. investigated the ferric salt effect on the adsorption of strong solid bases in order to determine the optimal FeO amount to increase the CO_2 capture in flue-gas at T > 150 °C. They synthesized the FeO–MgO using magnesium acetate and ferrous acetate. In particular, after grinding and carbonization treatments of the two salts at 550 °C, a composite FeO-MgO is obtained in which the ferric species are surrounded by magnesia particles with a surface area higher than 160 m^2 g^{-1}. Furthermore, with a 3% mass ratio of FeO the basic sorbent can capture 35 mg g^{-1} CO_2 at 150°. The CO_2 capture capacity and the ratio of strong basic sites results are higher than those of other MgO sorbents, resulting in an optimal situation for warm CO_2 capture [94].

3. Thermodynamics of Carbon Capture with Iron Oxides

In order to obtain low-cost iron products with high performances from natural iron ores, the reactions with reducing agents such as H_2 and CO need to be investigated in detail. The kinetics and thermodynamics of these reduction reactions will be discussed in the following chapter.

The reduction of Fe_2O_3 to the metallic iron (Fe) occurs stepwise. At temperatures > 570 °C, reduction is composed of three steps ($Fe_2O_3 \rightarrow Fe_3O_4 \rightarrow Fe_{(1-y)}O \rightarrow Fe$) according to the Equation (3a–c). At temperatures < 570 °C, Fe_2O_3 reduces firstly to Fe_3O_4 and then to Fe ($Fe_2O_3 \rightarrow Fe_3O_4 \rightarrow Fe$), according to the two-step reaction reported in Equation (4a,b), while the $Fe_{(1-y)}O$ intermediate is unstable.

$$3Fe_2O_3 + H_2 \rightarrow 2Fe_3O_4 + H_2O \; \mathbf{T} > 570\ ^\circ\mathrm{C} \quad (3a)$$

$$(1-y)Fe_3O_4 + (1-4y)H_2 \rightarrow 3Fe_{(1-y)}O + (1-4y)H_2O \quad (3b)$$

$$Fe_{(1-y)}O + H_2 \rightarrow (1-y)Fe + H_2O \quad (3c)$$

$$3Fe_2O_3 + H_2 \rightarrow 2Fe_3O_4 + H_2O, \; \mathbf{T} < 570\ ^\circ\mathrm{C} \quad (4a)$$

$$Fe_3O_4 + 4H_2 \rightarrow 3Fe + 4H_2O, \quad (4b)$$

The stability of different iron oxide forms can be analyzed by the diagram composed of temperature versus O (wt%/100) reported in Figure 1.

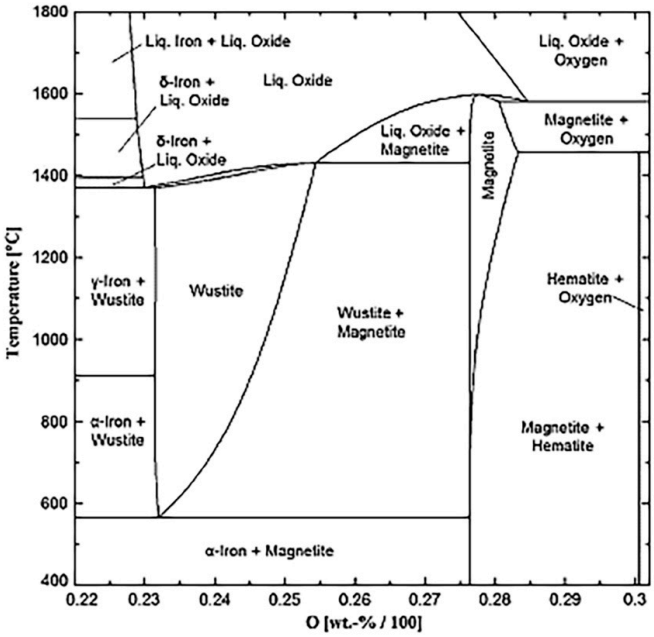

Figure 1. Binary system of Fe-O in which the effect of temperature versus O wt%/100 is reported. Reprinted from [95].

The oxygen-to-iron content in the Fe-based systems scales in the following order: Fe_2O_3 > Fe_3O_4 > FeO. As previously mentioned, FeO is stable at T > 570 °C while at T < 570 °C Fe_2O_3 decomposes to Fe_3O_4 and Fe. However, the FeO stability area expands by increasing the temperature, because not all places in the lattice are occupied by iron ions. For this reason, the FeO formula has to be considered as $Fe_{(1-y)}O$ in which 1−y represents vacancies in the iron lattice [96].

The Baur–Glässner diagram based on the thermodynamics of iron ore reduction is shown in Figure 2.

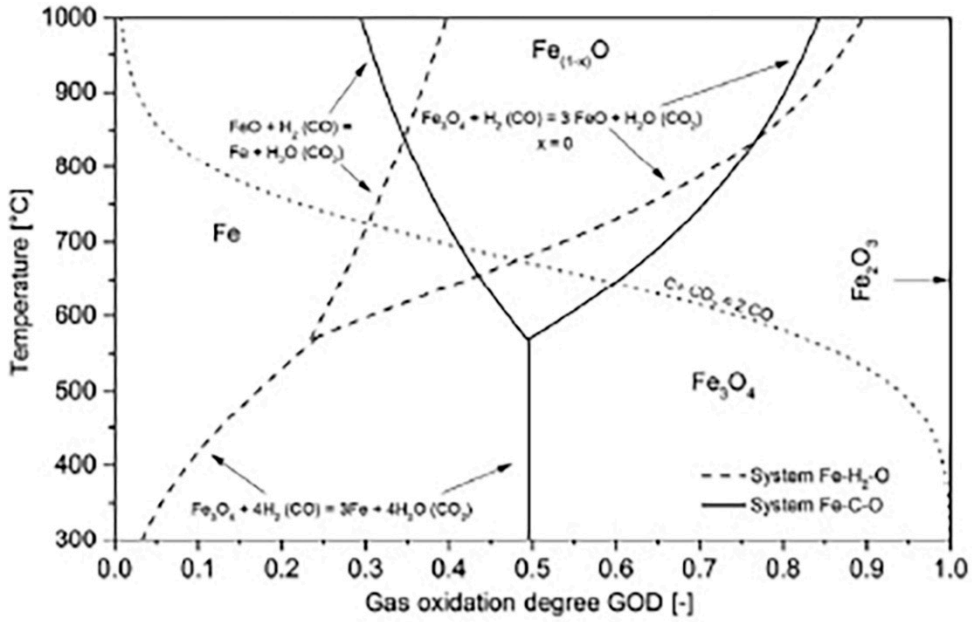

Figure 2. Baur–Glässner diagram for the Fe-O-H_2 and Fe-O-C system including the Boudouard equilibrium for 1 bar and a carbon activity of 1. Reprinted from [95].

In particular, the diagram describes the stability areas of the different iron oxide phases during the reaction with H_2 (continuous three-phase line) and with CO (dashed three-phase line) as a function of gas oxidation degree (GOD) and temperature [95,97]. The GOD value is determined as the ratio of oxidized gas components over the sum of oxidized and oxidizable gas components (e.g., for a CO-CO_2 mixture, GOD = CO/(CO + CO_2)) and is an indicator of the reduction force of a gas mixture (the lower the GOD, the higher the reduction force of the gas mixture). It is possible to note from the diagram that when reduction is carried out with H_2, the stability region of Fe increases with temperature and GOD. Contrariwise, when reduction is carried out with CO, Fe is never stable for GOD > 0.5 and the iron stability region decreases with temperature for GOD < 0.5.

Therefore, in order to achieve Fe with H_2 the temperature of reduction must be lowered as the GOD decreases. Instead, in order to achieve Fe with CO, GOD must be kept above 0.5 and the temperature of reduction must be increased as the GOD decreases. For the best possible gas utilization, it is therefore recommended to operate at high temperatures with H_2 and at low temperatures with CO.

For the Fe-C-O system, the Boudouard reaction, see Equation (5), must also be considered. For this reason, the corresponding equilibrium line (calculated assuming a carbon activity of 1 and a pressure of 1 bar) is also reported in the diagram.

$$2CO \rightleftarrows CO_2 + C \quad (5)$$

The Boudouard equilibrium line delimitates the Baur–Glässner diagram into two sections. For a CO-CO_2 gas mixture with composition and temperature below the equilibrium line, carbon precipitation can occur and hinder the reduction.

Furthermore, it is necessary to highlight that the reduction with CO is exothermic, while the reduction with H_2 is endothermic; therefore, in this case energy must be added to the system in order to maintain a constant reaction temperature. From an industrial point of view, an adequate process design, that involves the pre-heating of the materials, could aid in overcoming issues due to the supply of energy to the system [95].

4. Morphology and Microstructural Properties of Iron Oxides

Iron oxides involved in industrial processes and research activities have different features such as particle size, porosity, and purity degree. The true density of iron oxides

decreases in the order Fe > $Fe_{(1-y)}O$ > Fe_2O_3 > Fe_3O_4 (7.86 > 5.46 > 5.20 > 5.16 kg/m^3 [98]. However, bulk or apparent density depends on porosity. In several industrial applications cm-size pellets or briquettes are used, compacting finer grains, from tens of micrometers to a few millimeters in size. The interstices between the grains generate large macroporosity from micro to even millimetric scale, while pores inside the fine grains contribute with smaller (micro and mesopore) range porosity.

Hakim et al. investigated the microstructure of fine powders of different iron oxides by SEM, shown in Figure 3**.** In particular, a honeycomb structure can be observed for FeO, a rhombohedral lattice for Fe_2O_3, and a clear cubical structure for Fe_3O_4. In terms of porosity, the following average pore diameters (d_{pore}) and pore volumes (V_{pore}) are reported: d_{pore}= 62.5 nm and V_{pore} = 0.0003 cm^3/g for FeO; d_{pore} = 17.5 nm and V_{pore} = 0.029 cm^3/g for Fe_2O_3; and d_{pore} = 15.5 nm and V_{pore} = 0.018 cm^3/g for Fe_3O_4 [99].

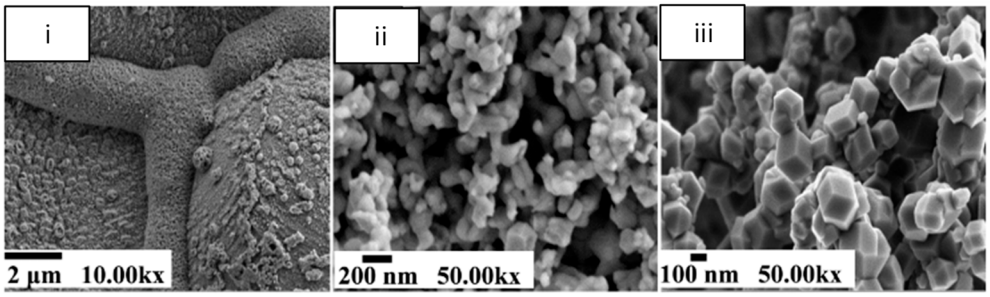

Figure 3. SEM micrographs of (**i**) FeO, (**ii**) Fe_2O_3, and (**iii**) Fe_3O_4. Reprinted from [99].

4.1. Porosity Changes in Reduction of Iron Ores

The porosity and density of the iron ore materials are key parameters controlling the reduction kinetics of the iron ore materials [100]. An analysis of the cross sections of large and hard particles after partial reduction reveals that reduction follows a topochemical pattern and concentric layers of different oxides are established, composed of Fe_2O_3, Fe_3O_4, $Fe_{(1-y)}O$ and Fe, respectively. Concentric layers are not observed for porous particles, yet a topochemical type of reduction could still be possible at a smaller scale, within the micro-grains which constitute larger pellets, Figure 4.

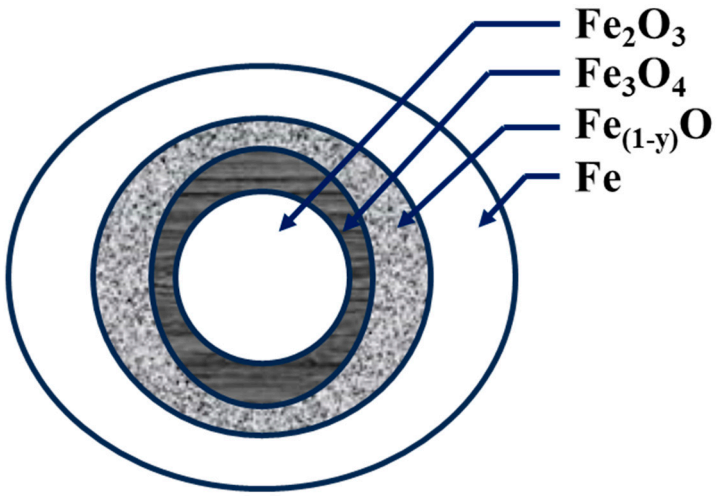

Figure 4. Representation of topochemical reduction of an iron ore particle.

In several papers, the mutual relationship between porosity and reduction rate or progress was addressed [96,101,102].

Ghadi et al. compared several pellets of iron ores and highlighted the porosity, grain size, and particle size effect and found that the rate of reduction increased linearly with the initial porosity degree of the samples, Figure 5 [103,104].

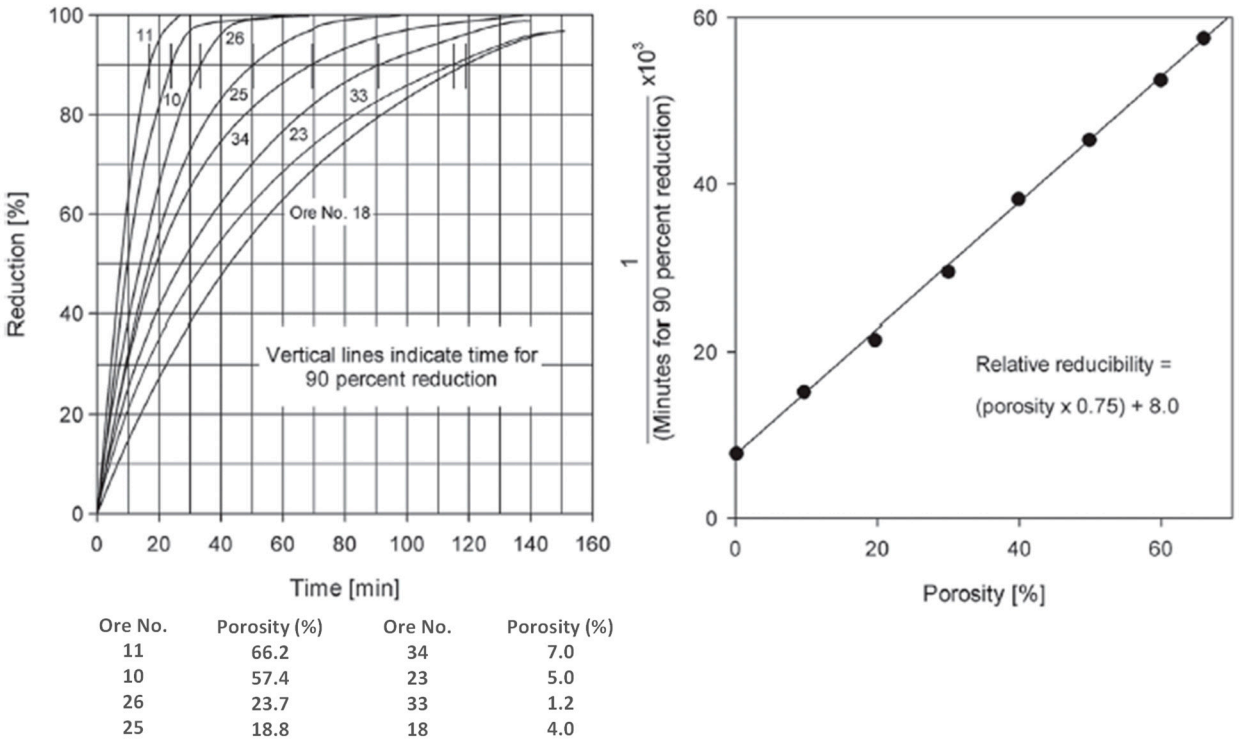

Ore No.	Porosity (%)	Ore No.	Porosity (%)
11	66.2	34	7.0
10	57.4	23	5.0
26	23.7	33	1.2
25	18.8	18	4.0

Figure 5. Pellet porosity effect on the rate of reduction for different iron ore samples. Reprinted from [104].

Sarkar et al. [100] reported, instead, for twenty different samples of Fe_2O_3 pellets (diameter 12 mm), a progressive decrease in porosity and increase in density upon reduction at 900 °C with CO and H_2.

El-Geassy et al. studied the effects of temperature on the structure of Fe_2O_3 pellets upon reduction with H_2 and reported different trends in the evolution of porosity, according to the compaction degree and grains particles size. Indeed, for the less porous/more compact pellets and larger grains size, high temperature and prolonged reduction treatments induce sintering, which reduces the reactivity of the samples [101]. On the other hand, for highly porous pellets and small grain sizes [105], sintering effects are less important, while the densification of the unreduced oxide grains results in an overall increase in porosity and reduction reactivity.

4.2. Effect of Gangue on Reduction Kinetics and Porosity

Iron ores also contain additional gangue, such as Al_2O_3, SiO_2, CaO, and MgO, in different amounts, depending on the ore and the enrichment process. In general, gangue can have a prominent effect on the reduction rate of iron oxides and on sintering [101].

Teplov et al. investigated the rate of reduction with H_2 of natural Fe_3O_4 concentrates in the range 300–570 °C and observed that stronger oxides, such as Al_2O_3, Ti_2O_3, V_2O_3, Mn_3O_4, and MgO, that form solid solutions with Fe_3O_4, decrease reduction rate, because they decrease the Gibbs thermodynamic potential and the equilibrium oxygen pressure over Fe_3O_4. Among these oxides, Al_2O_3 strongly decreases the rate of hydrogen reduction of Fe_3O_4, while MgO showed a weak effect [106].

Kapelyushin et al. investigated the effect of Al_2O_3 on the reactivity of iron ore reduction. In particular, they compared the reduction rate of undoped and doped Fe_3O_4 with CO-CO_2 gas mixtures at different temperatures. As shown in Figure 5 of [107], an amount of alumina, 3%, enhances the reduction reactivity of iron ore, but for higher amounts of alumina the effect is reversed and reduction rate decreases [107,108].

Paananen et al. also investigated the effect of alumina on Fe_3O_4 during reduction in a CO/CO_2 gas mixture at 850 °C and found that an Al-doped Fe_3O_4 sample reduces

more rapidly than the undoped Fe_3O_4 sample [109]. They attributed this to swelling and crack formation, suggesting that, upon doping, Al cations diffuse into the Fe_3O_4 structure forming hercynite. Upon reduction, high tension forces in the Fe_3O_4-hercynite phase close to the interface with the FeO would cause the disruption of the structure and generation of creaks.

As far as Ca is concerned, different papers addressed the effects of lime as well as of calcium carbonate on the reducibility of iron ores, and showed that their effect is beneficial, resulting in an enhancement of porosity upon reduction [101,110]. On the contrary, MgO would have a detrimental effect on iron reducibility [111]. As far as SiO_2 is concerned, controversial results have been reported in the literature; however, it seems that the effect of silica alone on the reduction reactivity of iron ores [112,113] can be considered of lower importance than that of other gangues, however SiO_2 can be involved in the formation of several phases when it is combined with Fe and Ca, such as in fayalite and calcio-ferrite.

4.3. Microstructural Changes in CO_2 Capture by Iron Oxides

The relation between microstructure and CO_2 captures by Fe_2O_3, Fe_3O_4, and FeO has been widely investigated in the literature [96,99,114].

Hakim et al. [99] investigated the microstructure and morphology of different iron oxides upon reaction with CO_2. In particular, they compared materials before and after CO_2 exposure for 4, 24, and 48 h and observed differences in carbonate growth on the surface, as shown in Figure 6.

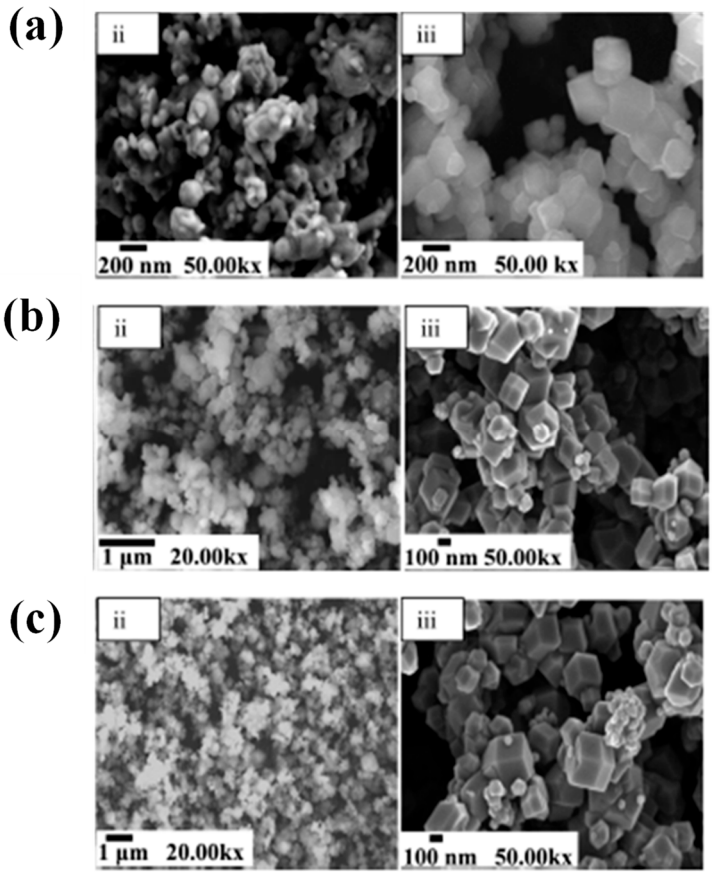

Figure 6. SEM micrographs for iron oxides treated with CO_2: (**a**) for 4 h; (**b**) for 24 h; and (**c**) for 48 h of Fe_2O_3, and Fe_3O_4. Reprinted from [99].

In particular, the formation of bicarbonate, monodentate carbonate, and bidentate carbonates, as well as the morphological changes of the iron particles were observed. For FeO, SEM micrographs highlighted the honeycomb structure that became smooth and groove-like upon exposure with CO_2, suggesting the chemical interaction of the iron

structure with several carbonate species. For Fe_3O_4 some sharp nanoparticles, indicative of carbonate formation, were clearly identified after exposure to CO_2; however, the cubic lattice of the iron oxide was preserved. A similar, but more remarkable effect was observed for Fe_3O_4, where nanoparticles form larger aggregates. Among all iron oxides, the uptake of CO_2 was consistently highest with Fe_2O_3 (at 3.01 $mgCO_2/g$).

5. Kinetics of Iron Ore Reduction

Several papers reported kinetic studies on iron ores reduction in different atmospheres. The majority, in fact, addressed the kinetics of reduction with H_2 and used thermogravimetric methods, either isothermal or non-isothermal. The results obtained are very scattered, as can be observed from the values of activation energies reported in Table 1, which indeed span between 57.1 (isothermal test) and 246 (non-isothermal test) kJ/mol. Kinetic models also spanned from simple first-order reactions to more complex models.

Table 1. Reduction of iron oxides by hydrogen with their amounts of apparent activation energy [95].

Operative Conditions	Reduction Reaction	E_a (kJ/mol)	Reference
Non-Isothermal with H_2	$Fe_2O_3 \rightarrow Fe_3O_4$ $Fe_3O_4 \rightarrow Fe$ $Fe_2O_3 \rightarrow Fe_3O_4$ $Fe_3O_4 \rightarrow Fe$	246 93.2 162.1 103.6	[115]
	$Fe_2O_3 \rightarrow Fe_3O_4$ $Fe_3O_4 \rightarrow FeO$ $FeO \rightarrow Fe$	139.2 77.3 85.7	[116]
	$Fe_2O_3 \rightarrow Fe_3O_4$ $Fe_3O_4 \rightarrow Fe$	89.1 70.4	[117]
	$FeO \rightarrow Fe$	104.0	[118]
Isothermal with H_2	$Fe_2O_3 \rightarrow Fe$ $Fe_2O_3 \rightarrow Fe$ $Fe_2O_3 \rightarrow Fe$	57.1 72.7 89.9	[119]
	$Fe_2O_3 \rightarrow Fe_3O_4$	30.1	[120]
	$Fe_2O_3 \rightarrow FeO$ $FeO \rightarrow Fe$	47.0 30.0	[121]
	$Fe_2O_3 \rightarrow Fe$ $Fe_2O_3 \rightarrow Fe$	47.2 51.5	[122]
	$Fe_2O_3 \rightarrow FeO$ $FeO \rightarrow Fe$	42.0 55.0	[123]
	$Fe_2O_3 \rightarrow FeO$ $FeO \rightarrow Fe$	33.0 11.0	[124]

Notably, the reliability of kinetic expressions obtained by conventional (thermogravimetric) methods for any heterogenous (gas–solid) reaction relies on the fulfilment of some conditions:

1. Reactions result in a single stage of mass loss or in well-resolved and defined sequential stages.
2. The structure of the solid reactant is relatively constant throughout the experiment.
3. Inter- and intra-particle mass and temperature diffusion resistances are negligible.

It is evident that, due to the complexity of its reaction scheme, the reduction of iron by hydrogen does not fulfil the first condition.

The second condition is not fulfilled either, because the reduction of iron oxides leads to different metallic iron formations (Fe_2O_3, Fe_3O_4, and FeO).

As for the third condition, the mass transfer limitation (of the gaseous reactants) can be avoided by performing experiments at low temperature and with fine particles; however,

in the reduction of iron ores, even for small particles size, an additional mechanism must be considered, that is, the transfer of electrons and iron ions generated by changes in iron oxides.

The complex interactions between physical and chemical phenomena and their impacts on the rate of the reaction of iron oxides with H_2/CO will be better explained in the following paragraph.

6. Effect of Physical and Chemical Phenomena on the Reaction Rate

The rate of reduction of iron ore particles depends on a complex series of chemical and transport phenomena, as reported in Scheme 1.

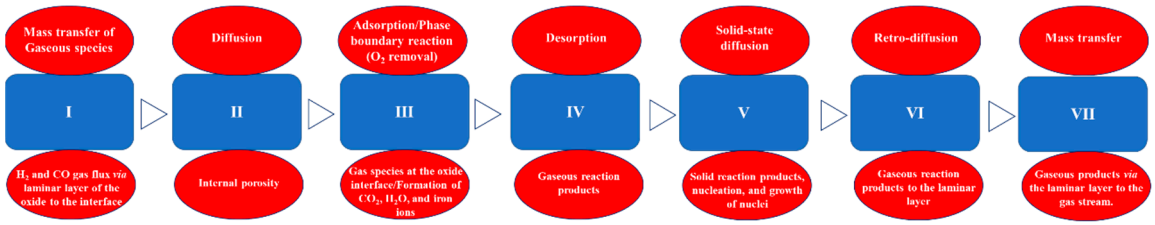

Scheme 1. Physical and chemical phenomena contributing to the reduction rate of porous iron ore particles.

The first step is the mass transfer of the reducing gas from the bulk of the gas phase to the particles' outer surface. This is followed by diffusion within pores and chemical reaction (including adsorption on the iron oxide internal surface and phase boundary reaction). Chemical reactions inside the particles produce gaseous products (CO_2 or H_2O), which have to diffuse towards the particle's outer surface, through particle pores. Electrons and iron ions generated by changes in iron oxides, instead, diffuse towards the particle's inner core by means of a solid-state diffusion mechanism. Reaction fronts and even concentrical layers of solid reduction products can therefore be established inside the particle as already shown in Figure 4 [125].

Notably, solid-state diffusion, which involves interstitial sites and defects, is much slower than gas diffusion and strongly dependent on the form of iron oxide. Gas transport in porous particles, instead, occurs through molecular diffusion mechanisms in pores with diameters larger than the mean free path, and according to a Knudsen diffusion mechanism in pores with diameters smaller than the mean free path [126].

As reported in previous paragraphs, reduction and heat treatment can progressively alter the porosity and microstructure of the material and modify the controlling reaction pattern. Two opposite phenomena are possible: on one side, the formation of creaks upon reduction can generate new porosity, which facilitates gas diffusion, and on the other side, sintering and the formation of dense iron layers reduces porosity and slows down gas diffusion.

Generally, in the literature, at least for fine particles [127–130], the first stage of reduction, $Fe_2O_3 \rightarrow Fe_3O_4$, is relatively fast and limited by gas diffusion, while the second stage of the reaction, whereby Fe_3O_4 is reduced to $Fe_{(1-y)}O$ or Fe, is slower and parameters such as temperature, concentration, particle size, and porosity all contribute to determine the rate-limiting step [123,124]. In particular, Table 2 reports a selection of experimental works that highlighted the rate-limiting process in the reduction of Fe_3O_4 to $Fe_{(1-y)}O$ or Fe for different particles typology (grains or pellets), size, morphology, and porosity, and for different process parameters such as temperature, pressure, and gas composition. Results are also summarized in Figure 7a, for the reaction with H_2 and H_2/CO mixtures, and in Figure 7b, for CO and CO/H_2 mixtures.

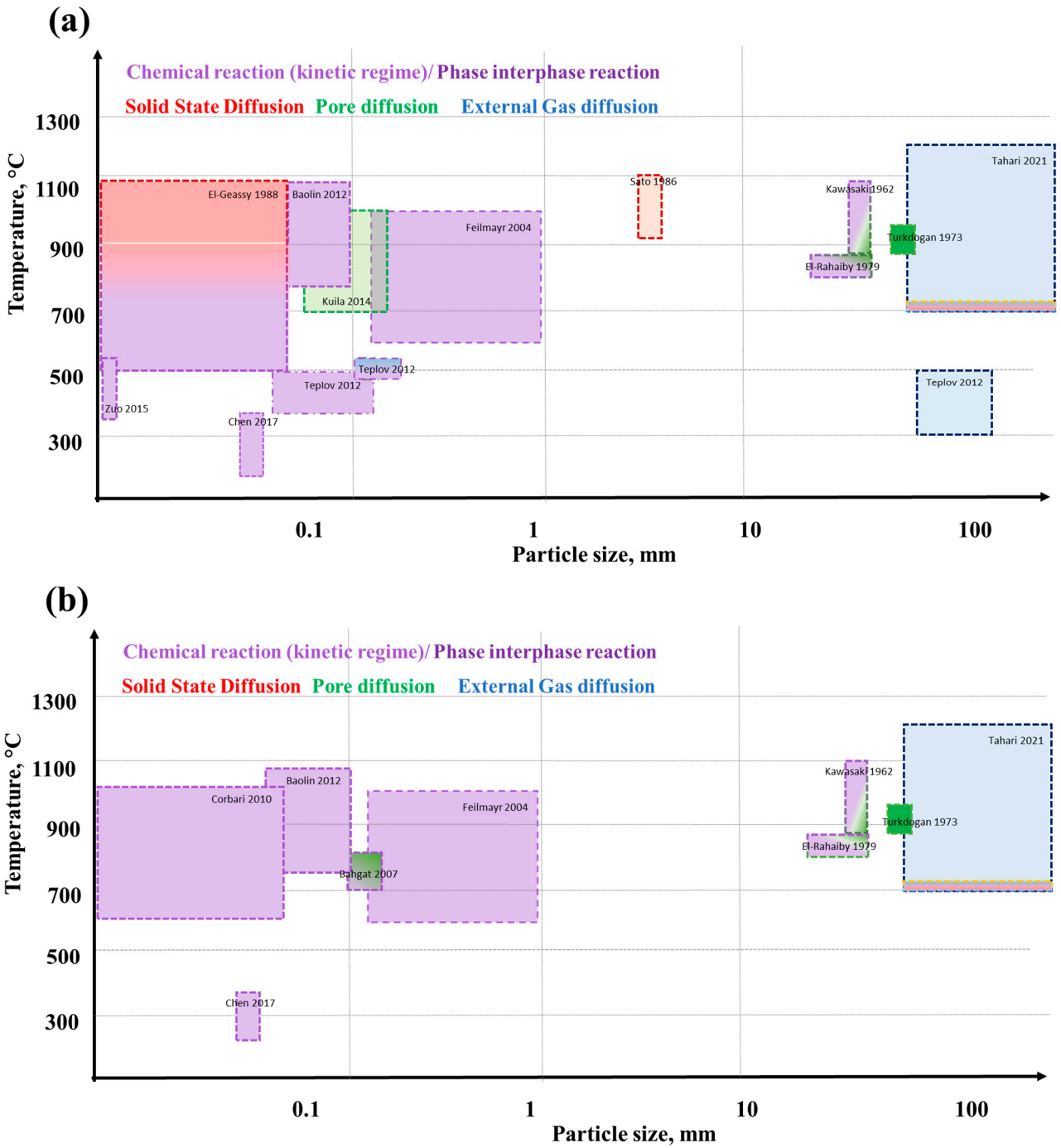

Figure 7. Experimental works on rate-limiting step in reduction of Fe_3O_4 to $Fe_{(1-y)}O$ or Fe for different parameters: (**a**) reaction with H_2 and H_2/CO mixtures [101,105,106,123,125,131–137] and (**b**) reaction with CO and CO/H_2 mixtures [101,125,130,131,133–135,138,139].

At high temperatures and for large particles size or large porosity, the rate-limiting step is generally external mass transfer. On the contrary, for low temperatures and fine particles size, intrinsic kinetics/phase boundary reaction controls the overall rate [140–142]. In intermediate cases, the controlling rate mechanism could be either gas or solid-state diffusion and even mixed regimes are possible where, for example, transport and phase boundary reaction have comparable relevance [106,132].

Table 2. The effect of different parameters on iron oxide reduction.

Reducing Agent	Particle Size	Porosity (ε)	T (°C)	P (bar)	E*a* (kJ/mol)	Limitation Steps (2nd Reaction Step)	Reference
H_2	4 mm × 4 mm × 8 mm	-	900–1100	-	99.2	Solid-state diffusion	[138]
H_2, CO	125 to 500 µm	0.15	350–600	10	91	Phase boundary reaction	[125]
CO	100–150 µm	-	700–850	-	80	Nucleation of FeO and then internal diffusion	[136]
H_2	<74 µm	0.54	500–1100	68	51 for T < 650 °C; 84 for 650–900 °C; 176 for T > 900 °C	T < 650 °C chemical reaction, 650–900 °C chemical reaction + solid state diffusion, T > 900 °C solid state diffusion	[105]
CO-CO_2 H_2	50.8 µm	0.0115	240–417	-	71	Phase boundary reaction	[134]
H_2/CO/ mixtures	1.07–1.24 cm	0.06	850	-	-	Mixed (chemical reaction + pore diffusion) at the beginning, pore diffusion at the end	[143]
H_2/CO	-	-	800–1000	-	48.64 with CO 63.19 with H_2	First phase boundary reaction, then pore diffusion and mixed regime (at 800 °C and 900 °C).	[144]
H_2	75–180 µm	0.27	700–1000	0.25–1	33	Pore diffusion	[123]
H_2/CO	-	-	150–900	-	-	Solid-state diffusion	[135]
H_2/CO	1.5–4.4 cm	0.31	700–1200	1–2	-	Gas diffusion At 700 °C in the late stages solid state diffusion	[133]
H_2 CO/CO_2	14 mm	-	900	-	-	Pore diffusion	[101]
H_2/CO	12 mm	-	800–1000	-	-	Chemical reaction at the beginning, pore diffusion at the end	[137]
H_2	50–160 µm	0.5	400	1	-	Chemical reaction	[106]
H_2	100–160 µm	0.5	500	1	-	External gas transport + chemical reaction	[106]
H_2	pellets	0.5	300–500	1	-	Transport in the external H_2O layer	[106]
CO-CO_2	~150 µm	0.69	590–1000	1	-	T < 700 °C, mixed control in the pores T > 700 °C external gas transport	[130]
CO-CO_2	150–500 µm	0.42	590–1000	1	-	Chemical reaction	[130]
CO-CO_2	<75 µm	0.23	590–1000	1	-	Chemical reaction	[130]

Table 2. *Cont.*

Reducing Agent	Particle Size	Porosity (ε)	T (°C)	P (bar)	E*a* (kJ/mol)	Limitation Steps (2nd Reaction Step)	Reference
H_2	0.249 µm	-	400–570		131.5 Fe_3O_4 → FeO 76.0 FeO → Fe	Chemical reaction	[131]
H_2 CO	<100 µm	-	800–1100	-	41.15 with H_2 54.19 with CO	Phase boundary reaction	[145]

Notably it has also been reported that the rate-controlling step can change throughout reduction because of changes in the microstructure of the particles [133,136,143,144]. Kawasaki et al. performed the reduction of porous Fe_2O_3 spherical pellets of a few centimeters in size in streams of pure H_2 or CO at temperatures between 700° and 1200 °C. At the higher temperature, the reduction rate was entirely diffusion controlled and a shell of reduction was clearly visible in sections of partially reduced specimens, which moved concentrically into the core of the samples. However at the lower reduction temperatures, $Fe_{(1-y)}O$ was trapped inside dense shells of iron impervious to the reducing gas and the reaction proceeded by solid-state diffusion [133].

Variations in the controlling regime were also observed for finer particles. Chen et al. studied the reduction kinetics of 100–150 µm Fe_2O_3 by CO between 700–850 °C and concluded that the initial stage the reduction process was controlled by the gas–solid reaction occurring at the Fe/FeO interface, but subsequently it was controlled by the nucleation of FeO, and finally by diffusion. Moreover, the reactions of Fe_2O_3 → FeO and FeO → Fe occurred simultaneously but with different time dependences [136].

The changes in reaction regimes throughout the reduction of iron ores can be explained considering that the true density of the different oxides decreases in the order Fe > $Fe_{(1-y)}O$ > Fe_2O_3 > Fe_3O_4 and that denser iron oxide forms imply slower diffusion [146–149].

Thermodynamic considerations, summarized in the Baur–Glässner diagram, shown in Figure 2, indicate that transition from Fe_3O_4 to the denser Fe and $Fe_{(1-y)}O$ occurs above a critical temperature, whose value, however, varies according to the reduction potential of the gaseous atmosphere (which is the inverse of the GOD reported in Figure 2). In CO/CO_2 mixtures, a transition occurs at a temperature of ~570 °C for GOD above 50%, while it occurs at 1000 °C above 30% of GOD transition. In H_2/H_2O mixtures for GOD above 20%, the transition occurs above ~570 °C. As far as the differences between H_2 and CO as reducing agents are concerned, it can be observed that H_2 and CO have the same reduction potential at ~810 °C, while at higher temperatures the reduction potential of H_2 is higher than that of CO, while the CO's reduction potential is higher than H_2's at low temperatures.

Several authors investigated different gas composition effects on the reduction rate of iron ores [104,150]. Turkdogan et al. highlighted that the reduction rate of iron ore pellets in H_2/CO mixtures increased with H_2 concentration, likely due to its better gas diffusivity [101]. Also, El-Geassy et al. found that for the reduction of FeO micropellets between 900 and 1100 °C, the rate increased with the percentage of H_2 in the gas mixture, and they observed a neat formation of Fe nuclei. On the contrary, when reduction was carried out with pure CO, they detected a delay in reduction resulting in an incubation time [151]. These results confirm that the thermodynamically driven changes of iron forms end up also having an impact on the reaction rate, because of the different densities of the iron forms that determine different diffusional resistances which might ultimately control the overall reaction rate.

In addition, the diffusivity of the reducing agent molecule should be considered.

Indeed, Zuo et al. investigated the reduction rate in a H_2/CO atmosphere at 800 °C, where the thermodynamic transition between more or less dense iron forms is comparable

for H_2 and CO, see Figure 3 of [137]. Even under these conditions, they observed that the reduction rate is higher with H_2, thanks to the better diffusivity of the H_2 molecule. They also conclude that increasing the CO amount, even by a small amount, in a gas mixture hinders the diffusion path of H_2 leading to an inhibition of the chemical reaction [137]. The decrease in the rate when CO is present in the reducing gas was also observed by El Geassy et al. who attributed it to a poisoning effect of CO molecules on the $Fe_{(1-y)}O$ surface [152].

7. Conclusions, Challenges and Future Perspectives

The use of iron-based materials for CO_2 capture is still under exploration; however, research executed in the last five years has shown that iron oxide materials could facilitate CO_2 capture thanks to their utilization directly in industrial plants. An interesting route for CO_2 capture, especially in the context of steel industry, is the reaction of Fe_2O_3 or Fe_3O_4 with reduced iron and with CO_2 to form $FeCO_3$. The CO_2, captured in the form of $FeCO_3$, can be easily transported by truck, and on a decarbonation stage, can free the CO_2 and regenerate iron.

While the main advantages of this route are clearly the large availability and relative cheapness of iron across the globe, a successful application of natural iron ores requires a careful analysis and comprehension of the relationships between their structural properties (density, porosity, etc.) and process conditions (temperature, gas composition). The pre-reduction step, necessary to reduce iron ores to metallic iron, may, in this respect, play a crucial role.

Luckily, a great deal of information on the microstructural properties of the different iron oxide forms and on the kinetics and thermodynamics of their reduction can be obtained from the large amount of literature which has been produced over the last decades in the context of steel making. The following general indications can be pointed out:

- H_2, for thermodynamic and kinetic reasons, is a better reduction agent than CO thanks to better diffusion behavior. Indeed, the viscosity and the molecule size of H_2 are lower than CO, affecting the diffusion behavior.
- The first step of reduction, leading from Fe_2O_3 to Fe_3O_4, below 570 °C, is relatively fast compared to further reduction from Fe_3O_4 to $Fe_{(1-y)}O$ or Fe; however, it is important because it opens up porosity.

The rate of reduction of Fe_3O_4 to $Fe_{(1-y)}O$ or Fe can be limited by structural features of the starting material and by microstructural changes occurring upon reduction and heat treatment. The rate-controlling step at high temperatures and for large particle size or large porosity is generally external gas transport. On the contrary, for low temperatures and finer particles size, solid-state diffusion or phase boundary reaction can hamper the overall rate.

It is clear from the current state-of-the-art that the best conditions for the production of iron-based materials, which are not only efficient in capturing CO_2, but that can also be re-used over several cycles, cannot be superficially selected and require a careful analysis of the material properties, like grain size, porosity, mineralogy, and the presence of gangue. Further research activity in this field is warmly encouraged to provide guidelines for the utilization of natural iron ores in CO_2 capture, as well as to unlock the potential of advances/engineered iron-based materials for CCS.

Author Contributions: A.F.: Conceptualization, Writing—original draft, Writing—review & editing. F.C.: Writing—original draft. O.S.: Conceptualization, Writing—original draft, Writing—review and editing, Supervision, and Funding Acquisition. All authors have read and agreed to the published version of the manuscript.

Funding: Antonio Fabozzi acknowledges funding from the European Union—NextGenerationEU under the National Recovery and Resilience Plan (PNRR), Mission 04 Component 2 Investment 3.1, and Project "ECCSELLENT—Development of ECCSEL-R.I. ItaLian facilities: usEr access, services and loNg-Term sustainability" Code: IR0000020—CUP F53C22000560006.

Data Availability Statement: Data are contained within the article.

Conflicts of Interest: The authors declare that they have no known competing financial interests or personal relationships that could have appeared to influence the work reported in this paper.

Abbreviations

Abbreviation	Name
CO_2	Carbon dioxide
Fe_2O_3	Hematite
Fe_3O_4	Magnetite
$Fe_{(1-y)}O$	Wüstite
IEA	International Energy Agency
H_2	Hydrogen
CO	Carbon oxide
CCS	Carbon Capture and Sequestration
EOR	Enhance Oil Recovery
CaO	Calcium oxides
TRL	Technology Readiness Level
N_2	Nitrogen
MgO	Magnesium oxides
CLC	Chemical Looping Combustion
$FeCO_3$	Siderite
MOFs	Metal organic frameworks
O_2	Oxygen
Al_2O_3	Alumina
SiO_2	Silica
Al	Aluminium
Fe	Iron
ATS	(3-Aminopropyl) triethoxysilane
TeOS	Tetraethyl orthosilicate
A	L (+)-ascorbic acid
C	Carbon
Mn	Manganese
Mn_3O_4	Hausmannite
CH_4	Methane
GOD	Gas Oxidation Degree
SEM	Scanning electron microscopy
d_{pore}	Pore diameter
V_{pore}	Pore volume
Ti_2O_3	Tistarite
V_2O_3	Karelianite
H_2O	Water

References

1. Yoro, K.O.; Daramola, M.O. CO_2 emission sources, greenhouse gases, and the global warming effect. In *Advances in Carbon Capture*; Elsevier: Amsterdam, The Netherlands, 2020; pp. 3–28.
2. Jeffry, L.; Ong, M.Y.; Nomanbhay, S.; Mofijur, M.; Mubashir, M.; Show, P.L. Greenhouse gases utilization: A review. *Fuel* **2021**, *301*, 121017. [CrossRef]
3. Joshi, R.; Singh, H. Carbon sequestration potential of disturbed and non-disturbed forest ecosystem: A tool for mitigating climate change. *Afr. J. Environ. Sci. Technol.* **2020**, *14*, 385–393.
4. Nica, A.; Popescu, A.; Ibanescu, D.-C. Human influence on the climate system. *Curr. Trends Nat. Sci.* **2019**, *8*, 209–215.
5. Saleh, T.A. Nanomaterials and hybrid nanocomposites for CO_2 capture and utilization: Environmental and energy sustainability. *RSC Adv.* **2022**, *12*, 23869–23888. [CrossRef] [PubMed]
6. Wani, O.A.; Kumar, S.S.; Hussain, N.; Wani, A.I.A.; Subhash, B.; Parvej, A.; Rashid, M.; Popescu, S.M.; Mansoor, S. Multi-scale processes influencing global carbon storage and land-carbon-climate nexus: A critical review. *Pedosphere* **2023**, *33*, 250–267. [CrossRef]
7. Gajdzik, B.; Sroka, W.; Vveinhardt, J. Energy Intensity of Steel Manufactured Utilising EAF Technology as a Function of Investments Made: The Case of the Steel Industry in Poland. *Energies* **2021**, *14*, 5152. [CrossRef]

8. Kim, J.; Sovacool, B.K.; Bazilian, M.; Griffiths, S.; Lee, J.; Yang, M.; Lee, J. Decarbonizing the iron and steel industry: A systematic review of sociotechnical systems, technological innovations, and policy options. *Energy Res. Soc. Sci.* **2022**, *89*, 102565. [CrossRef]
9. Pareek, A.; Dom, R.; Gupta, J.; Chandran, J.; Adepu, V.; Borse, P.H. Insights into renewable hydrogen energy: Recent advances and prospects. *Mater. Sci. Energy Technol.* **2020**, *3*, 319–327. [CrossRef]
10. Amin, M.; Shah, H.H.; Fareed, A.G.; Khan, W.U.; Chung, E.; Zia, A.; Farooqi, Z.U.R.; Lee, C. Hydrogen production through renewable and non-renewable energy processes and their impact on climate change. *Int. J. Hydrogen Energy* **2022**, *47*, 33112–33134. [CrossRef]
11. Berdysheva, S.; Ikonnikova, S. The energy transition and shifts in fossil fuel use: The study of international energy trade and energy security dynamics. *Energies* **2021**, *14*, 5396. [CrossRef]
12. Kober, T.; Schiffer, H.-W.; Densing, M.; Panos, E. Global energy perspectives to 2060–WEC's World Energy Scenarios 2019. *Energy Strategy Rev.* **2020**, *31*, 100523. [CrossRef]
13. Griffin, P.W.; Hammond, G.P. Industrial energy use and carbon emissions reduction in the iron and steel sector: A UK perspective. *Appl. Energy* **2019**, *249*, 109–125. [CrossRef]
14. Holappa, L. A general vision for reduction of energy consumption and CO_2 emissions from the steel industry. *Metals* **2020**, *10*, 1117. [CrossRef]
15. Budinis, S.; Krevor, S.; Mac Dowell, N.; Brandon, N.; Hawkes, A. An assessment of CCS costs, barriers and potential. *Energy Strategy Rev.* **2018**, *22*, 61–81. [CrossRef]
16. Van der Spek, M.; Roussanaly, S.; Rubin, E.S. Best practices and recent advances in CCS cost engineering and economic analysis. *Int. J. Greenh. Gas Control.* **2019**, *83*, 91–104. [CrossRef]
17. Jiang, K.; Ashworth, P. The development of Carbon Capture Utilization and Storage (CCUS) research in China: A bibliometric perspective. *Renew. Sustain. Energy Rev.* **2021**, *138*, 110521. [CrossRef]
18. Hussin, F.; Aroua, M.K. Recent trends in the development of adsorption technologies for carbon dioxide capture: A brief literature and patent reviews (2014–2018). *J. Clean. Prod.* **2020**, *253*, 119707. [CrossRef]
19. Snæbjörnsdóttir, S.Ó.; Sigfússon, B.; Marieni, C.; Goldberg, D.; Gislason, S.R.; Oelkers, E.H. Carbon dioxide storage through mineral carbonation. *Nat. Rev. Earth Environ.* **2020**, *1*, 90–102. [CrossRef]
20. Kelemen, P.; Benson, S.M.; Pilorgé, H.; Psarras, P.; Wilcox, J. An overview of the status and challenges of CO_2 storage in minerals and geological formations. *Front. Clim.* **2019**, *1*, 9. [CrossRef]
21. Ajayi, T.; Gomes, J.S.; Bera, A. A review of CO_2 storage in geological formations emphasizing modeling, monitoring and capacity estimation approaches. *Pet. Sci.* **2019**, *16*, 1028–1063. [CrossRef]
22. Herzog, H.J. Scaling up carbon dioxide capture and storage: From megatons to gigatons. *Energy Econ.* **2011**, *33*, 597–604. [CrossRef]
23. Fabozzi, A.; Della Sala, F.; di Gennaro, M.; Solimando, N.; Pagliuca, M.; Borzacchiello, A. Polymer based nanoparticles for biomedical applications by microfluidic techniques: From design to biological evaluation. *Polym. Chem.* **2021**, *12*, 6667–6687. [CrossRef]
24. Fabozzi, A.; Vitiello, R.; Krauss, I.R.; Iuliano, M.; De Tommaso, G.; Amoresano, A.; Pinto, G.; Paduano, L.; Jones, C.; Di Serio, M.; et al. Synthesis, Surface Properties, and Self-Aggregation Behavior of a Branched N,N-Dimethylalkylamine Oxide Surfactant. *J. Surfactants Deterg.* **2019**, *22*, 115–124. [CrossRef]
25. Fabozzi, A.; Krauss, I.R.; Vitiello, R.; Fornasier, M.; Sicignano, L.; King, S.; Guido, S.; Jones, C.; Paduano, L.; Murgia, S.; et al. Branched alkyldimethylamine oxide surfactants: An effective strategy for the design of high concentration/low viscosity surfactant formulations. *J. Colloid Interface Sci.* **2019**, *552*, 448–463. [CrossRef]
26. Scermino, L.; Fabozzi, A.; De Tommaso, G.; Valente, A.J.M.; Iuliano, M.; Paduano, L.; D'Errico, G. pH-responsive micellization of an amine oxide surfactant with branched hydrophobic tail. *J. Mol. Liq.* **2020**, *316*, 113799. [CrossRef]
27. Savignano, L.; Fabozzi, A.; Vitiello, R.; Fornasier, M.; Murgia, S.; Guido, S.; Guida, V.; Paduano, L.; D'Errico, G. Effect of tail branching on the phase behavior and the rheological properties of amine oxide/ethoxysulfate surfactant mixtures. *Colloids Surf. A-Physicochem. Eng. Asp.* **2021**, *613*, 126091.
28. Massarweh, O.; Abushaikha, A.S. A review of recent developments in CO_2 mobility control in enhanced oil recovery. *Petroleum* **2022**, *8*, 291–317. [CrossRef]
29. Wang, L.; Tian, Y.; Yu, X.; Wang, C.; Yao, B.; Wang, S.; Winterfeld, P.H.; Wang, X.; Yang, Z.; Wang, Y. Advances in improved/enhanced oil recovery technologies for tight and shale reservoirs. *Fuel* **2017**, *210*, 425–445. [CrossRef]
30. Vega, F.; Baena-Moreno, F.; Fernández, L.M.G.; Portillo, E.; Navarrete, B.; Zhang, Z. Current status of CO_2 chemical absorption research applied to CCS: Towards full deployment at industrial scale. *Appl. Energy* **2020**, *260*, 114313. [CrossRef]
31. Bui, M.; Adjiman, C.S.; Bardow, A.; Anthony, E.J.; Boston, A.; Brown, S.; Fennell, P.S.; Fuss, S.; Galindo, A.; Hackett, L.A. Carbon capture and storage (CCS): The way forward. *Energy Environ. Sci.* **2018**, *11*, 1062–1176.
32. Oschatz, M.; Antonietti, M. A search for selectivity to enable CO_2 capture with porous adsorbents. *Energy Environ. Sci.* **2018**, *11*, 57–70. [CrossRef]
33. Odunlami, O.; Vershima, D.; Oladimeji, T.; Nkongho, S.; Ogunlade, S.; Fakinle, B. Advanced techniques for the capturing and separation of CO_2—A review. *Results Eng.* **2022**, *15*, 100512. [CrossRef]
34. Salvi, B.L.; Jindal, S. Recent developments and challenges ahead in carbon capture and sequestration technologies. *SN Appl. Sci.* **2019**, *1*, 885. [CrossRef]

35. Madejski, P.; Chmiel, K.; Subramanian, N.; Kuś, T. Methods and techniques for CO_2 capture: Review of potential solutions and applications in modern energy technologies. *Energies* **2022**, *15*, 887. [CrossRef]
36. Mendoza, E.Y.M.; Santos, A.S.; López, E.V.; Drozd, V.; Durygin, A.; Chen, J.; Saxena, S.K. Iron oxides as efficient sorbents for CO_2 capture. *J. Mater. Res. Technol.* **2019**, *8*, 2944–2956. [CrossRef]
37. Ramirez-Vidal, P.; Sdanghi, G.; Celzard, A.; Fierro, V. High hydrogen release by cryo-adsorption and compression on porous materials. *Int. J. Hydrogen Energy* **2022**, *47*, 8892–8915. [CrossRef]
38. Nicotera, I.; Policicchio, A.; Conte, G.; Agostino, R.G.; Rehman, M.H.U.; Lufrano, E.; Simari, C. Quaternized polyepichlorohydrin-based membrane as high-selective CO_2 sorbent for cost-effective carbon capture. *J. CO_2 Util.* **2022**, *63*, 102135. [CrossRef]
39. Tao, H.; Qian, X.; Zhou, Y.; Cheng, H. Research progress of clay minerals in carbon dioxide capture. *Renew. Sustain. Energy Rev.* **2022**, *164*, 112536. [CrossRef]
40. Powell, C.E.; Qiao, G.G. Polymeric CO_2/N_2 gas separation membranes for the capture of carbon dioxide from power plant flue gases. *J. Membr. Sci.* **2006**, *279*, 1–49. [CrossRef]
41. Barbera, E.; Mio, A.; Pavan, A.M.; Bertucco, A.; Fermeglia, M. Fuelling power plants by natural gas: An analysis of energy efficiency, economical aspects and environmental footprint based on detailed process simulation of the whole carbon capture and storage system. *Energy Convers. Manag.* **2022**, *252*, 115072. [CrossRef]
42. Sanchez Moore, C.C.; Kulay, L. Effect of the implementation of carbon capture systems on the environmental, energy and economic performance of the Brazilian electricity matrix. *Energies* **2019**, *12*, 331. [CrossRef]
43. Dutcher, B.; Fan, M.; Russell, A.G. Amine-based CO_2 capture technology development from the beginning of 2013 A Review. *ACS Appl. Mater. Interfaces* **2015**, *7*, 2137–2148. [CrossRef] [PubMed]
44. Osman, A.I.; Hefny, M.; Abdel Maksoud, M.; Elgarahy, A.M.; Rooney, D.W. Recent advances in carbon capture storage and utilisation technologies: A review. *Environ. Chem. Lett.* **2021**, *19*, 797–849. [CrossRef]
45. Yamada, H. Amine-based capture of CO_2 for utilization and storage. *Polym. J.* **2021**, *53*, 93–102. [CrossRef]
46. Haaf, M.; Anantharaman, R.; Roussanaly, S.; Ströhle, J.; Epple, B. CO_2 capture from waste-to-energy plants: Techno-economic assessment of novel integration concepts of calcium looping technology. *Resour. Conserv. Recycl.* **2020**, *162*, 104973. [CrossRef]
47. Aghel, B.; Janati, S.; Wongwises, S.; Shadloo, M.S. Review on CO_2 capture by blended amine solutions. *Int. J. Greenh. Gas Control* **2022**, *119*, 103715. [CrossRef]
48. Ochedi, F.O.; Yu, J.; Yu, H.; Liu, Y.; Hussain, A. Carbon dioxide capture using liquid absorption methods: A review. *Environ. Chem. Lett.* **2021**, *19*, 77–109. [CrossRef]
49. Gür, T.M. Carbon dioxide emissions, capture, storage and utilization: Review of materials, processes and technologies. *Prog. Energy Combust. Sci.* **2022**, *89*, 100965. [CrossRef]
50. Siegelman, R.L.; Milner, P.J.; Kim, E.J.; Weston, S.C.; Long, J.R. Challenges and opportunities for adsorption-based CO_2 capture from natural gas combined cycle emissions. *Energy Environ. Sci.* **2019**, *12*, 2161–2173. [CrossRef]
51. Raganati, F.; Miccio, F.; Ammendola, P. Adsorption of carbon dioxide for post-combustion capture: A review. *Energy Fuels* **2021**, *35*, 12845–12868. [CrossRef]
52. Sifat, N.S.; Haseli, Y. A critical review of CO_2 capture technologies and prospects for clean power generation. *Energies* **2019**, *12*, 4143. [CrossRef]
53. Ramli, N.A.; Hashim, N.A.; Aroua, M.K. Prediction of CO_2/O_2 absorption selectivity using supported ionic liquid membranes (SILMs) for gas–liquid membrane contactor. *Chem. Eng. Commun.* **2018**, *205*, 295–310. [CrossRef]
54. da Silva Freitas, W.; Mecheri, B.; Vecchio, C.L.; Gatto, I.; Baglio, V.; Ficca, V.C.; Patra, A.; Placidi, E.; D'Epifanio, A. Metal-organic-framework-derived electrocatalysts for alkaline polymer electrolyte fuel cells. *J. Power Sources* **2022**, *550*, 232135. [CrossRef]
55. Ruhaimi, A.; Aziz, M.; Jalil, A. Magnesium oxide-based adsorbents for carbon dioxide capture: Current progress and future opportunities. *J. CO_2 Util.* **2021**, *43*, 101357. [CrossRef]
56. Dunstan, M.T.; Donat, F.; Bork, A.H.; Grey, C.P.; Müller, C.R. CO_2 capture at medium to high temperature using solid oxide-based sorbents: Fundamental aspects, mechanistic insights, and recent advances. *Chem. Rev.* **2021**, *121*, 12681–12745. [CrossRef] [PubMed]
57. Sun, H.; Wu, C.; Shen, B.; Zhang, X.; Zhang, Y.; Huang, J. Progress in the development and application of CaO-based adsorbents for CO_2 capture—A review. *Mater. Today Sustain.* **2018**, *1*, 1–27.
58. Abd, A.A.; Othman, M.R.; Kim, J. A review on application of activated carbons for carbon dioxide capture: Present performance, preparation, and surface modification for further improvement. *Environ. Sci. Pollut. Res.* **2021**, *28*, 43329–43364. [CrossRef] [PubMed]
59. André, L.; Abanades, S. Recent advances in thermochemical energy storage via solid–gas reversible reactions at high temperature. *Energies* **2020**, *13*, 5859. [CrossRef]
60. Jin, B.; Wei, K.; Ouyang, T.; Fan, Y.; Zhao, H.; Zhang, H.; Liang, Z. Chemical looping CO_2 capture and in-situ conversion: Fundamentals, process configurations, bifunctional materials, and reaction mechanisms. *Appl. Energy Combust. Sci.* **2023**, *16*, 100218. [CrossRef]
61. Goyal, P.; Tiwary, C.S.; Misra, S.K. Ion exchange based approach for rapid and selective Pb (II) removal using iron oxide decorated metal organic framework hybrid. *J. Environ. Manag.* **2021**, *277*, 111469. [CrossRef]
62. Zhang, X.; Jiao, K.; Zhang, J.; Guo, Z. A review on low carbon emissions projects of steel industry in the World. *J. Clean. Prod.* **2021**, *306*, 127259. [CrossRef]

63. Chai, W.S.; Cheun, J.Y.; Kumar, P.S.; Mubashir, M.; Majeed, Z.; Banat, F.; Ho, S.-H.; Show, P.L. A review on conventional and novel materials towards heavy metal adsorption in wastewater treatment application. *J. Clean. Prod.* **2021**, *296*, 126589. [CrossRef]
64. Taghizadeh, S.-M.; Berenjian, A.; Zare, M.; Ebrahiminezhad, A. New perspectives on iron-based nanostructures. *Processes* **2020**, *8*, 1128. [CrossRef]
65. Hamza, A.; Hussein, I.A.; Jalab, R.; Saad, M.; Mahmoud, M. Review of iron sulfide scale removal and inhibition in oil and gas wells: Current status and perspectives. *Energy Fuels* **2021**, *35*, 14401–14421. [CrossRef]
66. Garibello, C.F.; Eldridge, D.S.; Malherbe, F.; Hocking, R.K. Abiotic transformations of nitrogen mediated by iron sulfides and related species from early Earth to catalyst design. *Inorg. Chem. Front.* **2023**, *10*, 6792–6811. [CrossRef]
67. Ubando, A.T.; Chen, W.H.; Show, P.L.; Ong, H.C. Kinetic and thermodynamic analysis of iron oxide reduction by graphite for CO_2 mitigation in chemical-looping combustion. *Int. J. Energy Res.* **2020**, *44*, 3865–3882. [CrossRef]
68. Abuelgasim, S.; Wang, W.; Abdalazeez, A. A brief review for chemical looping combustion as a promising CO_2 capture technology: Fundamentals and progress. *Sci. Total Environ.* **2021**, *764*, 142892. [CrossRef] [PubMed]
69. Raganati, F.; Alfe, M.; Gargiulo, V.; Chirone, R.; Ammendola, P. Kinetic study and breakthrough analysis of the hybrid physical/chemical CO_2 adsorption/desorption behavior of a magnetite-based sorbent. *Chem. Eng. J.* **2019**, *372*, 526–535. [CrossRef]
70. Manchisi, J.; Matinde, E.; Rowson, N.A.; Simmons, M.J.; Simate, G.S.; Ndlovu, S.; Mwewa, B. Ironmaking and steelmaking slags as sustainable adsorbents for industrial effluents and wastewater treatment: A critical review of properties, performance, challenges and opportunities. *Sustainability* **2020**, *12*, 2118. [CrossRef]
71. Gaikwad, S.; Kim, Y.; Gaikwad, R.; Han, S. Enhanced CO_2 capture capacity of amine-functionalized MOF-177 metal organic framework. *J. Environ. Chem. Eng.* **2021**, *9*, 105523. [CrossRef]
72. Hussein, A.; Burra, K.; Bassioni, G.; Hammouda, R.; Gupta, A. Production of CO from CO_2 over mixed-metal oxides derived from layered-double-hydroxides. *Appl. Energy* **2019**, *235*, 1183–1191. [CrossRef]
73. Chandrasekaran, S.; Bowen, C.; Zhang, P.; Li, Z.; Yuan, Q.; Ren, X.; Deng, L. Spinel photocatalysts for environmental remediation, hydrogen generation, CO_2 reduction and photoelectrochemical water splitting. *J. Mater. Chem. A* **2018**, *6*, 11078–11104. [CrossRef]
74. Nikolaeva, N.V.; Aleksandrova, T.N.; Chanturiya, E.L.; Afanasova, A. Mineral and technological features of magnetite–hematite ores and their influence on the choice of processing technology. *ACS Omega* **2021**, *6*, 9077–9085. [CrossRef] [PubMed]
75. Cabello, A.; Abad, A.; García-Labiano, F.; Gayán, P.; De Diego, L.; Adánez, J. Kinetic determination of a highly reactive impregnated Fe_2O_3/Al_2O_3 oxygen carrier for use in gas-fueled Chemical Looping Combustion. *Chem. Eng. J.* **2014**, *258*, 265–280. [CrossRef]
76. Enoch, K.; Sundaram, A.; Ponraj, S.S.; Sathya, P.; George, S.D.B.; Kumar, M.R. Enhancement of MXene optical properties towards medical applications via metal oxide incorporation. *Nanoscale* **2023**, *15*, 16874–16889. [CrossRef]
77. Zhang, S.; Saha, C.; Yang, Y.; Bhattacharya, S.; Xiao, R. Use of Fe_2O_3-containing industrial wastes as the oxygen carrier for chemical-looping combustion of coal: Effects of pressure and cycles. *Energy Fuels* **2011**, *25*, 4357–4366. [CrossRef]
78. Gu, H.; Shen, L.; Xiao, J.; Zhang, S.; Song, T. Chemical looping combustion of biomass/coal with natural iron ore as oxygen carrier in a continuous reactor. *Energy Fuels* **2011**, *25*, 446–455. [CrossRef]
79. Song, T.; Shen, T.; Shen, L.; Xiao, J.; Gu, H.; Zhang, S. Evaluation of hematite oxygen carrier in chemical-looping combustion of coal. *Fuel* **2013**, *104*, 244–252. [CrossRef]
80. Pawar, A.A.; Bandal, H.A.; Kim, H. Spinel type Fe_3O_4 polyhedron supported on nickel foam as an electrocatalyst for water oxidation reaction. *J. Alloys Compd.* **2021**, *863*, 158742. [CrossRef]
81. Santos-Carballal, D.; Roldan, A.; Dzade, N.Y.; De Leeuw, N.H. Reactivity of CO_2 on the surfaces of magnetite (Fe_3O_4), greigite (Fe_3S_4) and mackinawite (FeS). *Philos. Trans. R. Soc. A Math. Phys. Eng. Sci.* **2018**, *376*, 20170065. [CrossRef]
82. Zhu, H.; Ren, X.; Yang, X.; Liang, X.; Liu, A.; Wu, G. Fe-based catalysts for nitrogen reduction toward ammonia electrosynthesis under ambient conditions. *SusMat* **2022**, *2*, 214–242. [CrossRef]
83. Raza, S.; Orooji, Y.; Ghasali, E.; Hayat, A.; Karimi-Maleh, H.; Lin, H. Engineering approaches for CO_2 converting to biomass coupled with nanobiomaterials as biomediated towards circular bioeconomy. *J. CO_2 Util.* **2023**, *67*, 102295. [CrossRef]
84. Shan, J.; Wang, L.; Yu, H.; Ji, J.; Amer, W.; Chen, Y.; Jing, G.; Khalid, H.; Akram, M.; Abbasi, N. Recent progress in Fe_3O_4 based magnetic nanoparticles: From synthesis to application. *Mater. Sci. Technol.* **2016**, *32*, 602–614. [CrossRef]
85. Park, J.H.; Lee, J.W.; Ahn, H.; Kang, Y.T. Development of novel nanoabsorbents by amine functionalization of Fe_3O_4 with intermediate ascorbic acid coating for CO_2 capture enhancement. *J. CO_2 Util.* **2022**, *65*, 102228. [CrossRef]
86. Yu, W.; Wang, T.; Park, A.-H.A.; Fang, M. Review of liquid nano-absorbents for enhanced CO_2 capture. *Nanoscale* **2019**, *11*, 17137–17156. [CrossRef] [PubMed]
87. Kluytmans, J.; Van Wachem, B.; Kuster, B.; Schouten, J. Mass transfer in sparged and stirred reactors: Influence of carbon particles and electrolyte. *Chem. Eng. Sci.* **2003**, *58*, 4719–4728. [CrossRef]
88. Li, L.; Kang, Y.T. Enhancement mechanisms of mass transfer performance by nanoabsorbents during CO_2 absorption process. *Int. J. Heat Mass Transf.* **2021**, *164*, 120444. [CrossRef]
89. Kars, R.; Best, R.; Drinkenburg, A. The sorption of propane in slurries of active carbon in water. *Chem. Eng. J.* **1979**, *17*, 201–210. [CrossRef]
90. Kim, W.-g.; Kang, H.U.; Jung, K.-m.; Kim, S.H. Synthesis of silica nanofluid and application to CO_2 absorption. *Sep. Sci. Technol.* **2008**, *43*, 3036–3055. [CrossRef]

91. Li, L.; Kang, Y.T. Effects of bubble coalescence and breakup on CO_2 absorption performance in nanoabsorbents. *J. CO_2 Util.* **2020**, *39*, 101170. [CrossRef]
92. Abad, A.; de Las Obras-Loscertales, M.; García-Labiano, F.; de Diego, L.; Gayán, P.; Adánez, J. In situ gasification Chemical-Looping Combustion of coal using limestone as oxygen carrier precursor and sulphur sorbent. *Chem. Eng. J.* **2017**, *310*, 226–239. [CrossRef]
93. Pérez-Vega, R.; Abad, A.; Gayán, P.; de Diego, L.; García-Labiano, F.; Adánez, J. Development of $(Mn_{0.77}Fe_{0.23})_2O_3$ particles as an oxygen carrier for coal combustion with CO_2 capture via in-situ gasification chemical looping combustion (iG-CLC) aided by oxygen uncoupling (CLOU). *Fuel Process. Technol.* **2017**, *164*, 69–79. [CrossRef]
94. Chen, J.L.; Dong, X.Y.M.; Shi, C.L.; Li, S.H.; Wang, Y.; Zhu, J.H. Fabrication of strong solid base FeO–MgO for warm CO_2 capture. *CLEAN–Soil Air Water* **2019**, *47*, 1800447. [CrossRef]
95. Spreitzer, D.; Schenk, J. Reduction of iron oxides with hydrogen—A review. *Steel Res. Int.* **2019**, *90*, 1900108. [CrossRef]
96. Kim, S.-H.; Zhang, X.; Ma, Y.; Souza Filho, I.R.; Schweinar, K.; Angenendt, K.; Vogel, D.; Stephenson, L.T.; El-Zoka, A.A.; Mianroodi, J.R. Influence of microstructure and atomic-scale chemistry on the direct reduction of iron ore with hydrogen at 700 C. *Acta Mater.* **2021**, *212*, 116933. [CrossRef]
97. Cavaliere, P. Hydrogen Ironmaking. In *Hydrogen Assisted Direct Reduction of Iron Oxides*; Springer: Berlin/Heidelberg, Germany, 2022; pp. 131–183.
98. Akiyama, T.; Ohta, H.; Takahashi, R.; Waseda, Y.; Yagi, J.-I. Measurement and modeling of thermal conductivity for dense iron oxide and porous iron ore agglomerates in stepwise reduction. *ISIJ Int.* **1992**, *32*, 829–837. [CrossRef]
99. Hakim, A.; Marliza, T.S.; Abu Tahari, N.M.; Wan Isahak, R.W.; Yusop, R.M.; Mohamed Hisham, W.M.; Yarmo, A.M. Studies on CO_2 adsorption and desorption properties from various types of iron oxides (FeO, Fe_2O_3, and Fe_3O_4). *Ind. Eng. Chem. Res.* **2016**, *55*, 7888–7897. [CrossRef]
100. Sarkar, A.; Chavan, V.; Pai, N.; Prakash, A.; Hazra, B.; Raut, P.; Sunilkumar, D.; Sivananda, C.; Kundu, S.; Nag, S. Reduction of Iron Ore Pellets: A Microstructural Perspective? *Metall. Mater. Trans. A* **2023**, *55*, 537–549. [CrossRef]
101. Forsmo, S.; Forsmo, S.-E.; Samskog, P.-O.; Björkman, B. Mechanisms in oxidation and sintering of magnetite iron ore green pellets. *Powder Technol.* **2008**, *183*, 247–259. [CrossRef]
102. Zare Ghadi, A.; Valipour, M.S.; Vahedi, S.M.; Sohn, H.Y. A review on the modeling of gaseous reduction of iron oxide pellets. *Steel Res. Int.* **2020**, *91*, 1900270. [CrossRef]
103. Turkdogan, E.; Vinters, J. Reducibility of iron ore pellets and effect of additions. *Can. Metall. Q.* **1973**, *12*, 9–21. [CrossRef]
104. Hayes, P. The kinetics of formation of H_2O and CO_2 during iron oxide reduction. *Metall. Trans. B* **1979**, *10*, 211–217. [CrossRef]
105. Joseph, T. Porosity, reducibility and size preparation of iron ores. *Trans. AIME* **1936**, *120*, 72–89.
106. El-Geassy, A.; Nasr, M. Influence of the original structure on the kinetics of hydrogen reduction of hematite compacts. *Trans. Iron Steel Inst. Jpn.* **1988**, *28*, 650–658. [CrossRef]
107. Teplov, O. Kinetics of the low-temperature hydrogen reduction of magnetite concentrates. *Russ. Metall. (Met.)* **2012**, *2012*, 8–21. [CrossRef]
108. Kapelyushin, Y.; Xing, X.; Zhang, J.; Jeong, S.; Sasaki, Y.; Ostrovski, O. Effect of alumina on the gaseous reduction of magnetite in CO/CO_2 gas mixtures. *Metall. Mater. Trans. B* **2015**, *46*, 1175–1185. [CrossRef]
109. Kapelyushin, Y.; Sasaki, Y.; Zhang, J.; Jeong, S.; Ostrovski, O. Formation of a network structure in the gaseous reduction of magnetite doped with alumina. *Metall. Mater. Trans. B* **2017**, *48*, 889–899. [CrossRef]
110. Paananen, T.; Heinänen, K.; Härkki, J. Degradation of iron oxide caused by alumina during reduction from magnetite. *ISIJ Int.* **2003**, *43*, 597–605. [CrossRef]
111. Pal, J. Innovative development on agglomeration of iron ore fines and iron oxide wastes. *Miner. Process. Extr. Metall. Rev.* **2018**, *40*, 248–264. [CrossRef]
112. Cores, A.; Babich, A.; Muñiz, M.; Ferreira, S.; Mochon, J. The influence of different iron ores mixtures composition on the quality of sinter. *ISIJ Int.* **2010**, *50*, 1089–1098. [CrossRef]
113. Hsieh, L.-H.; JA, W. Effect of oxygen potential on mineral formation in lime-fluxed iron ore sinter. *ISIJ Int.* **1989**, *29*, 625–634. [CrossRef]
114. Mazanek, E.; Wyderko, M. Zur Optimierung der Eigenschaften von Eisenerzsintern. *Arch. Für Das Eisenhüttenwesen* **1976**, *47*, 457–463. [CrossRef]
115. Li, J.; Zhang, H.; Gao, Z.; Fu, J.; Ao, W.; Dai, J. CO_2 capture with chemical looping combustion of gaseous fuels: An overview. *Energy Fuels* **2017**, *31*, 3475–3524. [CrossRef]
116. Munteanu, G.; Ilieva, L.; Andreeva, D. TPR data regarding the effect of sulfur on the reducibility of α-Fe_2O_3. *Thermochim. Acta* **1999**, *329*, 157–162. [CrossRef]
117. Munteanu, G.; Ilieva, L.; Andreeva, D. Kinetic parameters obtained from TPR data for α-Fe_2O_3 and Auα-Fe_2O_3 systems. *Thermochim. Acta* **1997**, *291*, 171–177. [CrossRef]
118. Lin, H.-Y.; Chen, Y.-W.; Li, C. The mechanism of reduction of iron oxide by hydrogen. *Thermochim. Acta* **2003**, *400*, 61–67. [CrossRef]
119. Jozwiak, W.; Kaczmarek, E.; Maniecki, T.; Ignaczak, W.; Maniukiewicz, W. Reduction behavior of iron oxides in hydrogen and carbon monoxide atmospheres. *Appl. Catal. A Gen.* **2007**, *326*, 17–27. [CrossRef]

120. Sastri, M.; Viswanath, R.; Viswanathan, B. Studies on the reduction of iron oxide with hydrogen. *Int. J. Hydrogen Energy* **1982**, *7*, 951–955. [CrossRef]
121. Abd Elhamid, M.; Khader, M.; Mahgoub, A.; El Anadouli, B.; Ateya, B. Autocatalytic reduction of hematite with hydrogen under conditions of surface control: A vacancy-based mechanism. *J. Solid State Chem.* **1996**, *123*, 249–254. [CrossRef]
122. Barde, A.A.; Klausner, J.F.; Mei, R. Solid state reaction kinetics of iron oxide reduction using hydrogen as a reducing agent. *Int. J. Hydrogen Energy* **2016**, *41*, 10103–10119. [CrossRef]
123. Lee, G.-Y.; Choi, J.-P.; Song, J.-I.; Jung, S.-S.; Lee, J.-S. The kinetics of isothermal hydrogen reduction of nanocrystalline Fe_2O_3 powder. *Mater. Trans.* **2014**, *55*, 1611–1617. [CrossRef]
124. Kuila, S.K.; Chaudhuri, S.; Chatterjee, R.; Ghosh, D. In Reduction of magnetite ore fines with hydrogen. In Proceedings of the 4th International Conference on Chemical Engineering, Dhaka, Bangladesh, 29–30 December 2014; Chemical Engineering Department, BUET: Dhaka, Bangladesh, 2014; p. 81.
125. Kuila, S.K.; Chatterjee, R.; Ghosh, D. Kinetics of hydrogen reduction of magnetite ore fines. *Int. J. Hydrogen Energy* **2016**, *41*, 9256–9266. [CrossRef]
126. Feilmayr, C.; Thurnhofer, A.; Winter, F.; Mali, H.; Schenk, J. Reduction behavior of hematite to magnetite under fluidized bed conditions. *ISIJ Int.* **2004**, *44*, 1125–1133. [CrossRef]
127. Swimm, K.; Reichenauer, G.; Vidi, S.; Ebert, H.-P. Gas pressure dependence of the heat transport in porous solids with pores smaller than 10 µm. *Int. J. Thermophys.* **2009**, *30*, 1329–1342. [CrossRef]
128. Du, Z.; Liu, J.; Liu, F.; Pan, F. Relationship of particle size, reaction and sticking behavior of iron ore fines toward efficient fluidized bed reduction. *Chem. Eng. J.* **2022**, *447*, 137588. [CrossRef]
129. Komatina, M.; Gudenau, H.W. The sticking problem during direct reduction of fine iron ore in the fluidized bed. *Metall. Mater. Eng.* **2018**. [CrossRef] [PubMed]
130. Chung, U.-C.; Lee, I.-O.; Kim, H.-G.; Sahajwalla, V.; Chung, W.-B. Degradation characteristics of iron ore fines of a wide size distribution in fluidized-bed reduction. *ISIJ Int.* **1998**, *38*, 943–952. [CrossRef]
131. Corbari, R.; Fruehan, R. Reduction of iron oxide fines to wustite with CO/CO_2 gas of low reducing potential. *Metall. Mater. Trans. B* **2010**, *41*, 318–329. [CrossRef]
132. Gudenau, H. *Materialsammlung Zum Praktikum Metallurgie*; Trans-Aix-Press: Aachen, Germany, 2002.
133. Qu, Y.; Xing, L.; Shao, L.; Luo, Y.; Zou, Z. Microstructural characterization and gas-solid reduction kinetics of iron ore fines at high temperature. *Powder Technol.* **2019**, *355*, 26–36. [CrossRef]
134. Wolfinger, T.; Spreitzer, D.; Zheng, H.; Schenk, J. Influence of a prior oxidation on the reduction behavior of magnetite iron ore ultra-fines using hydrogen. *Metall. Mater. Trans. B* **2022**, *53*, 14–28. [CrossRef]
135. Sato, K.; Ueda, Y.; Nishikawa, Y.; Goto, T. Effect of Pressure on Reduction Rate of Iron Ore with High Pressure Fluidized Bed. *Trans. Iron Steel Inst. Jpn.* **1986**, *26*, 697–703. [CrossRef]
136. Bahgat, M.; Khedr, M. Reduction kinetics, magnetic behavior and morphological changes during reduction of magnetite single crystal. *Mater. Sci. Eng. B* **2007**, *138*, 251–258. [CrossRef]
137. Chen, H.; Zheng, Z.; Chen, Z.; Yu, W.; Yue, J. Multistep reduction kinetics of fine iron ore with carbon monoxide in a micro fluidized bed reaction analyzer. *Metall. Mater. Trans. B* **2017**, *48*, 841–852. [CrossRef]
138. El-Rahaiby, S.; Rao, Y. The kinetics of reduction of iron oxides at moderate temperatures. *Metall. Trans. B* **1979**, *10*, 257–269. [CrossRef]
139. Bonalde, A.; Henriquez, A.; Manrique, M. Kinetic analysis of the iron oxide reduction using hydrogen-carbon monoxide mixtures as reducing agent. *ISIJ Int.* **2005**, *45*, 1255–1260. [CrossRef]
140. Liu, D.; Wang, X.; Zhang, J.; Liu, Z.; Jiao, K.; Liu, X.; Wang, R. Study on the controlling steps and reduction kinetics of iron oxide briquettes with CO-H_2 mixtures. *Metall. Res. Technol.* **2017**, *114*, 611. [CrossRef]
141. Tahari, M.N.A.; Salleh, F.; Saharuddin, T.S.T.; Samsuri, A.; Samidin, S.; Yarmo, M.A. Influence of hydrogen and carbon monoxide on reduction behavior of iron oxide at high temperature: Effect on reduction gas concentrations. *Int. J. Hydrogen Energy* **2021**, *46*, 24791–24805. [CrossRef]
142. Kawasaki, E.; Sanscrainte, J.; Walsh, T.J. Kinetics of reduction of iron oxide with carbon monoxide and hydrogen. *AIChE J.* **1962**, *8*, 48–52. [CrossRef]
143. Zuo, H.-B.; Wang, C.; Dong, J.-J.; Jiao, K.-X.; Xu, R.-S. Reduction kinetics of iron oxide pellets with H_2 and CO mixtures. *Int. J. Miner. Metall. Mater.* **2015**, *22*, 688–696. [CrossRef]
144. Baolin, H.; Zhang, H.; Hongzhong, L.; Qingshan, Z. Study on kinetics of iron oxide reduction by hydrogen. *Chin. J. Chem. Eng.* **2012**, *20*, 10–17.
145. Hammam, A.; Li, Y.; Nie, H.; Zan, L.; Ding, W.; Ge, Y.; Li, M.; Omran, M.; Yu, Y. Isothermal and non-isothermal reduction behaviors of iron ore compacts in pure hydrogen atmosphere and kinetic analysis. *Min. Metall. Explor.* **2021**, *38*, 81–93. [CrossRef]
146. Moradmand, S.; Allen, J. Magnetic carbon formation via in-situ CO_2 capture and electrolysis in a molten carbonate system. *Mater. Today Sustain.* **2024**, *25*, 100645. [CrossRef]
147. Ouyang, T.; Jin, B.; Mao, Y.; Wei, D.; Liang, Z. Control of strong electronic oxide-support interaction in iron-based redox catalysts for highly efficient chemical looping CO_2 conversion. *Appl. Catal. B Environ.* **2024**, *343*, 123531. [CrossRef]
148. Rao, Q.; Zhang, J.; Yang, T.; Li, Y.; Gai, Z.; Li, P.; Wang, X.; Pan, Y.; Jin, H. A nickel-modified perovskite-supported iron oxide oxygen carrier for chemical looping dry reforming of methane for syngas production. *Chem. Eng. J.* **2024**, *485*, 150033. [CrossRef]

149. Saqline, S.; Wang, H.; Fan, Q.; Donat, F.; Müller, C.; Liu, W. Investigation of barium iron oxides for CO_2 capture and chemical looping oxygen uncoupling. *Appl. Energy Combust. Sci.* **2024**, *17*, 100238. [CrossRef]
150. Guo, D.; Hu, M.; Pu, C.; Xiao, B.; Hu, Z.; Liu, S.; Wang, X.; Zhu, X. Kinetics and mechanisms of direct reduction of iron ore-biomass composite pellets with hydrogen gas. *Int. J. Hydrogen Energy* **2015**, *40*, 4733–4740. [CrossRef]
151. El-Geassy, A.A.; Rajakumar, V. Gaseous reduction of wustite with H_2, CO and H_2-CO mixtures. *Trans. Iron Steel Inst. Jpn.* **1985**, *25*, 449–458. [CrossRef]
152. El-Geassy, A.-H.A. *In Rate Controlling Step in the Reduction of Iron Oxides; Kinetics and Mechanism of Wüstite-Iron Step in H_2, CO and H_2/CO Gas Mixtures*; IOP Conference Series: Materials Science and Engineering, 2017; IOP Publishing: Bristol, UK, 2017; p. 012002.